Fibers and Polymers (2023) 24:3913–3926
https://doi.org/10.1007/s12221-023-00341-2

Online ISSN 1875-0052
Print ISSN 1229-9197

REGULAR ARTICLE

Excellency of *Calendula arvensis* in AgNPs Synthesis for Cotton Fabrics in Terms of Shape Diversity and Antibacterial Wash Fastness

Toufique Ahmed[1] · **R. Tugrul Ogulata**[2] · **Osman Gülnaz**[3]

Received: 20 February 2023 / Revised: 1 August 2023 / Accepted: 17 August 2023 / Published online: 8 September 2023

Abstract

Green synthesis is a widely known silver nanoparticle (AgNPs) synthesis method. Hundreds of biological extracts have been applied for synthesizing of AgNPs. This study used *C. reticulata*, *C. sativus* and *C. arvensis* as plant extracts for AgNPs synthesis. It depicted the supremacy of *C. arvensis* in green synthesis. Here, we compared the nanoparticle's morphology and antibacterial activity of *C. arvensis* synthesized AgNPs with other previously accomplished works on different plant extracts. The AgNPs were incorporated in cotton fabrics with multiple methods. We used FTIR, UV–Vis, SEM, EDS, XRD, antibacterial activity, and wash fastness for characterization. The SEM image shows *C. arvensis* plant can synthesize different shapes, whereas *C. reticulata* synthesizes nearly spherical shapes. It also showed the *C. arvensis* plant extract exhibited 96% antibacterial activity after 20 washes with double padding methods, which is the best among the available works on antibacterial wash fastness without any binder or cross-linkers. In contrast, *Citrus reticulata* showed 88% antibacterial activity after five washes.

Keywords Silver nanoparticle · Green synthesis · Antimicrobial textiles · Antibacterial wash fastness

1 Introduction

Antimicrobial textiles are attaining prompt popularity. The Covid-19 pandemic, in particular, has accelerated the antimicrobial textile market demand. Various types of antimicrobial agents are available in the market such as quaternary ammonium compounds (QAC), triclosan, chitosan, polyhexamethylene biguanide (PHMB) etc. But these materials cause detrimental effect on skin, toxic to the animals, and hazardous. In comparison with other antibacterial agents, silver nitrate is comparatively safer. It is harmless for human health but highly toxic to bacteria [1]. Silver can inhibit more than 7 fungi species and 16 bacterial species [2]. For this reason, silver-based compounds have a potentially wide range of application domains such as food packaging, wound dressing, medical equipment, paints, etc.

Silver nitrate ($AgNO_3$) is one of the most common antimicrobial agents and it has been used for a prolonged period of time for this purpose. The Ag^+ released from $AgNO_3$ is mainly responsible for the antimicrobial properties of $AgNO_3$, which is comparatively nontoxic to humans and animals but toxic to viruses, bacteria, and fungi. But $AgNO_3$ needs a higher concentration to work against microbes. In converse, synthesis of silver nanoparticle requires a low concentrate $AgNO_3$ [3, 4]. Due to its large surface area-to-volume ratio, silver nanoparticles (AgNPs) are an excellent and safer alternative to other traditional antimicrobial agents [5]. Unlike other antimicrobial agents, it is the least detrimental to human health and the environment [1]. Various silver compounds, such as silver nitrate ($AgNO_3$), silver sulfate (Ag_2SO_4), etc. can produce silver nanoparticles. However, silver nitrate is more efficient in this context [6].

Nanoparticles can be synthesized in mainly two ways- (1) bottom-up (chemical methods) and (2) top-down (physical methods) [7]. The physical method has high energy

✉ Toufique Ahmed
tahmed@niter.edu.bd

R. Tugrul Ogulata
ogulata@cu.edu.tr

Osman Gülnaz
ogulnaz@cu.edu.tr

[1] Textile Engineering Department, National Institute of Textile Engineering and Research, Dhaka, Bangladesh

[2] Textile Engineering Department, Cukurova University, Adana, Turkey

[3] Department of Mathematics and Science Education, Faculty of Education, Cukurova University, Adana, Turkey

consumption, low production, imperfection, etc. On the other hand, chemical methods are cost-effective. Still, it requires two types of chemicals to reduce metal ions and stabilization, which may not be eco-friendly, sometimes toxic, and prone to produce hazardous by-products [8]. On the contrary, green synthesis is simple and cost-effective, and no additional chemical is needed. The plant extract can simultaneously handle the reduction, aggregation, and stabilization [9]. Moreover, it provides extraordinary assembly [10]. For green synthesis, many biological substances, such as plants, fungi, bacteria, yeast, etc., are used [11]. The biological substances contain various natural bioactive compounds such as flavonoids, polysaccharides, terpenoids, alkaloids, saponins, polyphenols, etc. [12]. These compounds cause the reduction of silver ions (Ag^+) to Ag atoms [6].

Vankar and Shukla [13] synthesized AgNPs from lemon leaves and 0.002 M $AgNO_3$ and found multi-shaped AgNPs. Awwad, Salem, and Abdeen [14] synthesized 5–40 nm sized AgNPs from carob leaves and 0.001 M $AgNO_3$. Maghimaa and Alharbi [15] utilized *Curcuma longa* to synthesize and load silver nanoparticles (AgNPs) into cotton fabric for antibacterial and wound-healing properties. The synthesized AgNPs can be incorporated into fabrics by ex-situ (coating, padding, spray, etc.) and in-situ methods [16]. But, the incorporated AgNPs tend to leach out from the fabric in most cases, to prevent leaching binder or cross-linkers are needed [17]. For example, Hebeish et al. [18] used a binder to increase wash fastness of AgNPs incorporated fabrics and found high wash fastness up to 20 wash cycles. On the other hand, some researchers claimed in-situ method increased AgNPs wash fastness, such as Tang et al. [19] incorporated AgNPs into mercerized and scoured cotton fabrics by in-situ method and found 100% antibacterial properties after seven washes. Again, Zhou et al. [20] incorporated Aloe vera synthesized AgNPs into cotton fabrics by in-situ method and reported substantial antibacterial activity up to 20 washes. In this study, we focused on increasing the wash fastness of AgNPs loaded cotton fabrics without using any binder or cross-linkers. In this effort, we reviewed numerous available studies and selected *Calendula arvensis* (field marigold), *Citrus reticulata* (mandarin orange), and *Cucumis sativus* (cucumber). No works were reported on these three plant extracts for antibacterial applications in textiles. However, Ituen et al. [21] synthesized AgNPs from *C. reticulata* peel extracts for anticorrosion and antibacterial performance and Hussain et al. [22] used green synthesized AgNPs to profile the biochemical of *C. reticulata*.

The reasons behind choosing these plant extracts are their availability, deficiency of previous works, presence of a wide range of bioactive phytochemicals etc. For example, *C. sativus* contains cucumerin A and B, orientin, cucurbitacins, cucumegastigmanes I and II, Isoscoparin, vitex, glucoside, apigenin [23]. *C. reticulata* has flavanones, flavones, flavonoids, hesperidin and vitamin C, naringenin, nobiletin, polymethoxyflavones (PMF), phenolic compounds, hesperidin, naringin, tangeretin, and rutin [24, 25]. However, *C. arvensis* was a little bit special to us as it is a well-known medicinal plant.

Generally, *C. arvensis* grows in empty fields, roadsides, rocky hillsides, cultivated fields, etc. Geographically these are available around Mediterranean coastal regions, including Turkey, southern Europe, Caucasia, Iran, and Afghanistan. The *Calendula* genus includes approximately 25 annual or perennial herbs [26]. Among them, three species are the most common. *Calendula arvensis Linn.*, *Calendula officinalis Linn.,* and *Calendula suffruticosa Vahl.* [27]. Among these 3 species, *C. officinalis* was used for silver nanoparticles (AgNPs) synthesis by various researchers. Rodríguez-Acosta et al. [28] utilized *C. officinalis* extract from drug delivery. Baghizadeh et al. [29] synthesized AgNPs from the seed extract of *Calendula officinalis* and found 5–10 nm sized spherical AgNPs with 4 months stability. Balciunaitiene et al. [30] compared *Calendula officinalis* (Calendula) *and* Hyssopus officinalis (Hyssopus) and found AgNPs synthesized by *C. officinalis* (35.7 ± 4.8 nm) are comparatively bigger than Hyssopus synthesized AgNPs (16.8 ± 5.8 nm) but the antibacterial activity of *C. officinalis* synthesized AgNPs is slightly better.

On the contrary, not many studies have been reported on green synthesis of AgNPs using *Calendula arvensis*. Toufique et. al. [31] reported an exceptional behavior of recovering antibacterial property loss- where the antibacterial efficiency of unused *C. arvensis* synthesized AgNPs incorporated cotton fabrics temporarily decreased at a large scale but was able to recover 100% antibacterial property while washed with detergent. *Calendula arvensis* has various properties such as antibacterial, anti-mutagenic, anti-inflammatory, antioxidant, hemolytic, etc. [32]. Paolini et al. [33] identified 85 essential oil components, including monoterpene, Sesquiterpene, alcohol, aldehyde, ketones, and esters from *C. arvensis*. Abutaha et al. [32] demonstrated that it could destroy breast cancer cells. *C. arvensis* is traditionally used as a spicy, food color, tea, ointment, tincture, and cosmetic cream [34]. Phytochemical studies showed that *C. arvensis* contains phenolic acids and flavonoids like different chemical compounds [35]. The presence of different types of phytochemicals indicates a very good potential

source for silver nanoparticles synthesis. For example, flavonoids reduce the metal ion and phenolic acids stabilized the synthesized AgNPs [11].

This study aims to synthesize AgNPs from *C. reticulata, C. sativus, and C. arvensis* extracts, and compare their morphological and antibacterial, and wash fastness. A comparative study was also made among different previously reported green synthesized AgNPs.

2 Materials and Methods

2.1 Materials

Silver nitrate (purity 99%), NaOH, Muller Hinton agar, and nutrient broth were supplied by Merck, Germany. The bacteria were collected from the microbiology laboratory of the university. The cotton fabrics (plain, GSM 123) were collected in a grey state without any pretreatments from a local textile factory.

2.2 Plant Extract Preparations

The *Calendula arvensis* (field marigold) plants were collected from the open field of Adana province in Turkey, *Citrus reticulata* (mandarin orange) and *Cucumis sativus* (cucumber) were collected from the University agricultural products sell center. Then the leaves of *C. arvensis* and peels of mandarin orange and cucumber were separated and placed in three separate beakers. Next, each plant sample was washed with 95% ethanol and dried at shade for a few days. The dried plant samples were chopped separately into small pieces. Next, 2.5 g of each plant sample was boiled in 150 ml water at 90 °C for 30 min individually. In this way, each plant sample produced a 90 ml solution. After returning back to room temperature, the solutions were filtered with a Whatman no. 1 filter paper. The three resultant solutions were collected in glass bottles and labeled according to the plant extract names. Finally, these were stored at a 3 °C for future use as a reducing and capping agent.

2.3 AgNPs Synthesis

We found temperature is a crucial factor for *C. arvensis* plant extract. The AgNPs could not be synthesized using *C. arvensis* plant extract at below 40 °C, and the stability and reaction rate is different from 40 to 70 °C for both $AgNO_3$ and Plant extract. Hence, we used Taguchi Orthogonal array to determine the optimum temperature for $AgNO_3$ and plant extract which is discussed in result and discussion section.

First, 100 ml $AgNO_3$ solution with different molarity, such as 0.002 M, 0.009 M, and 0.001 M was taken in a 500 ml Erlenmeyer flask and heated at 60 °C. In another beaker, the plant extract was also heated up to 55 °C. Then 4 drops (1/7 ml) of plant extract were added to the $AgNO_3$ solution. It took 6–8 min to change the color. The produced AgNPs suspension was used for padding and immersion. Besides, the required amount of $AgNO_3$, plant extract, and temperature was noted carefully and used in the *in-situ* silver nanoparticle synthesis.

2.4 AgNPs Loading in Cotton Fabrics

First, we cut the cotton fabric by 8 cm × 8 cm. Then, the samples were scoured with 4 gm/l NaOH at 90 °C for 1 h and boiled with distilled water for 1 h at 80 °C to reduce the alkalinity. Then, the silver nanoparticles were incorporated into the fabrics by padding, immersion, and in-situ method.

In padding method, the fabric samples were fully immersed in 100 ml previously synthesized silver nanoparticles (AgNPs) suspension and then padded with a padding machine (Rapid, Labortex) with 2 kg/cm^2 padding pressure to ensure 80% wet pick-up. The padded samples are then placed in an incubator at 60 °C for 30 min to dry. Next, the dried padded samples were washed with distilled water and dried at 70 °C for 10 min in an air drying cabinet.

In immersion method, the samples were immersed in 100 ml AgNPs suspension solution and waited for half an hour to impregnate. Then the samples were dried in an incubator at 60 °C and washed with distilled water. Finally, the samples were dried in an air drying cabinet at 70 °C for 10 min.

On the other hand, in the in-situ method, the fabric samples were immersed in $AgNO_3$ solution. Subsequently, the silver nitrate-soaked fabrics were introduced into a plant extract-reducing bath having pH 5–6 with 3:1 liquor-to-fabric ratio and kept overnight at room temperature. Then the fabrics were dried at 60 °C in a laboratory oven incubator. Finally, the fabric samples were washed with distilled water and dried in an air drying cabinet at 70 °C for 10 min.

2.5 Wash Fastness

The wash fastness of the AgNPs incorporated fabrics was done according to AATCC 61-2010 standard. Here, 4 g

AATCC standard reference detergent without any optical brighter was added to 120 ml water. The prepared solution (120 ml) was poured in the vessels, followed by the fabric samples were kept inside the vessels. Finally, the vessels were placed in the GyroWash machine (James Heal). The machine was run for 45 min at 40 °C with 10 steel balls. In this method, one wash cycle is equivalent to 5 home laundry.

2.6 Characterization of AgNPs

2.6.1 UV–Vis Spectroscopy

The Silver nanoparticles (AgNPs) synthesis was confirmed by UV–Vis Spectrophotometer (Shimadzu, UV-1800) with a wavelength range of 300–650 nm. Distilled water was used as a blank solution.

2.6.1.1 FTIR The chemical polymeric components of the samples were evaluated by Fourier-transform infrared spectroscopy (FTIR-6700, Jasco) through the spectral range 4000–400 cm^{-1}.

2.6.2 X-Ray Diffraction Measurements

The AgNPs treated cotton fabrics samples were used to measure X-ray diffraction (XRD). The samples were placed in XRD with EMPYRREAN diffractometer system (PANalytical EMPYREAN, Netherlands) with CuKα, wavelength $\lambda = 1.$ 540,598 Å. The scan range (2θ) was 10° to 90° and scanning step of 0.013. The tube voltage was 40 kV, and the tube current was 40 mA with Cu anode. Finally, HighScore plus was used to identify the peaks.

2.6.3 SEM and EDS

The morphology of AgNPs on cotton fabrics were observed by using SEM (FEI, Quanta 650, USA). First, the AgNPs loaded cotton fabric samples were coated with gold (Au) using a vacuum sputter coater. Then, the gold coated samples were used for SEM images. The accelerating voltage was 5.00 kV for different kinds of magnification starting from 20,000 to 100,000. After having the SEM image we used ImageJ software to determine the size of each nanoparticles in nanometer. Then the mean of all sizes were calculated. Besides, the elemental analysis of the samples was done using energy dispersive X-ray spectroscopy (EDS).

2.6.4 Antibacterial Activity

The antibacterial tests were done according to the AATCC-100 test standards using *S. aureus* (Gram-positive bacteria) and *K. pneumoniae* (Gram-negative bacteria) with a slight modification. A 4.8 cm × 4.8 cm square fabric sample was used in this method. First, an inoculum with 100 ml nutrient broth was incubated for 24 h at 37 °C. The concentration of bacteria should be 2×10^5 cells/ ml. Subsequently, about 1 ml of this inoculum was absorbed by each fabric sample. Then, each sample was incubated at 37 °C for 24 h. After the incubation period, 100 ml of water was added as a buffer solution, and the samples were mixed well by shaking. Serial dilution was performed to get the number of living bacteria. The process was repeated three times. Finally, the following formula calculates the percentage of bacterial reduction after 24 h incubation period:

$$\text{Reduction rate}\,\% = \frac{B - A}{B} \times 100$$

where B is the bacterial colony for the untreated sample, A is the bacterial colony for AgNPs treated sample.

3 Results and Discussions

This study found a significant effect on AgNPs synthesis and stability. *C. arvensis* plant extract failed to form silver nanoparticles below 40 °C. Hence, we synthesized AgNPs at different temperatures ranging from 40 to 70 °C and evaluated the particle formation by UV–Vis spectroscopy. Taguchi orthogonal array was used to find out the optimum temperature. Here, the temperature of $AgNO_3$ and the temperature of plant extract were regarded as two factors; each factor has four levels (40 °C, 50 °C, 60 °C, 70 °C). Hence, L_{16} (4^2) orthogonal array was selected to decide the optimum temperature. Table 1 depicts the L_{16} orthogonal array.

The contour plots in Fig. 1 show the result of the Taguchi orthogonal array. The optimum temperature for $AgNO_3$ and plant extract should be around 55 °C and 56–70 °C, respectively.

Therefore, the temperature was set to 55 °C for plant extract and 60 °C for $AgNO_3$ solution.

3.1 Mechanism of In-Situ Synthesis

The detailed mechanism of ex-situ synthesis has been described by T. Ahmed and Ogulata [9]. Here, we are focusing only on the in-situ mechanism. The hypothesized mechanism of entire in-situ green synthesis method is depicted in Fig. 2. Here, three significant steps are reduction, nucleation, and capping or stabilization. Most plant extracts can accomplish all three tasks simultaneously.

Table 1 L_{16} orthogonal design, levels of the factors, and experimental results

Exp. no.	Coded matrix		Actual matrix		Experimental results	
	A	*B*	$AgNO_3$ temp (ºC)	Plant extract temp (ºC)	UV vis SPR (nm)	Time (min)
1	1	1	70	70	421	3
2	1	2	70	60	422	1
3	1	3	70	50	421	4
4	1	4	70	40	420	4
5	2	1	60	70	425	14
6	2	2	60	60	417	14
7	2	3	60	50	423	12
8	2	4	60	40	423	12
9	3	1	50	70	424	36
10	3	2	50	60	416	26
11	3	3	50	50	424	42
12	3	4	50	40	425	42
13	4	1	40	70	416	180
14	4	2	40	60	424	180
15	4	3	40	50	424	180
16	4	4	40	40	424	180

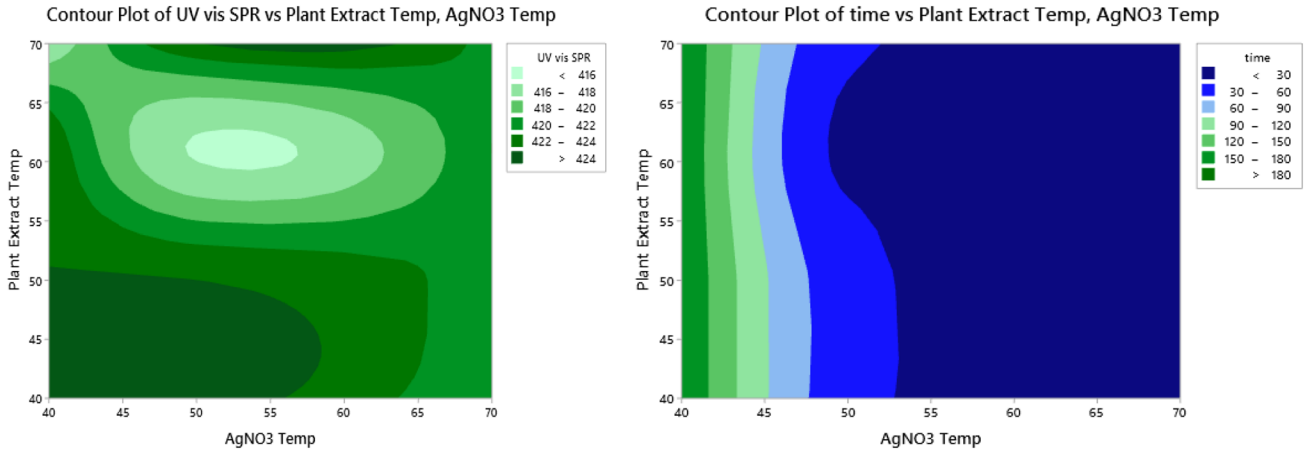

Fig. 1 Contour plots **a** UV-Vis SPR, **b** reaction time

First, Ag^+ ions from $AgNO_3$ get reduced by the co-enzymes (such as $NADP^+$ or NAD^+) present in the biological extract. The co-enzymes carry hydrogen atoms (H) with two electrons as NADPH/NADH. Later, the NADPH/NADH donates the electrons to the silver ions [36, 37].

$$NAD^+ + H^+ \rightarrow NADH - 2e^-$$

$$Ag^+ + e^- \rightarrow Ag$$

Then, the newly formed Ag atoms get nucleated to form nanoparticles. This freshly formed nanoparticles develops new volume and consequently creates free energy. This free energy initiates the nucleation process. In this way, the smaller particles begin to grow swiftly due to their high free energy [38]. Hence it must be stopped; otherwise, the large particle will become larger, whereas smaller particles will be diminishing through the Ostwald ripening [39].

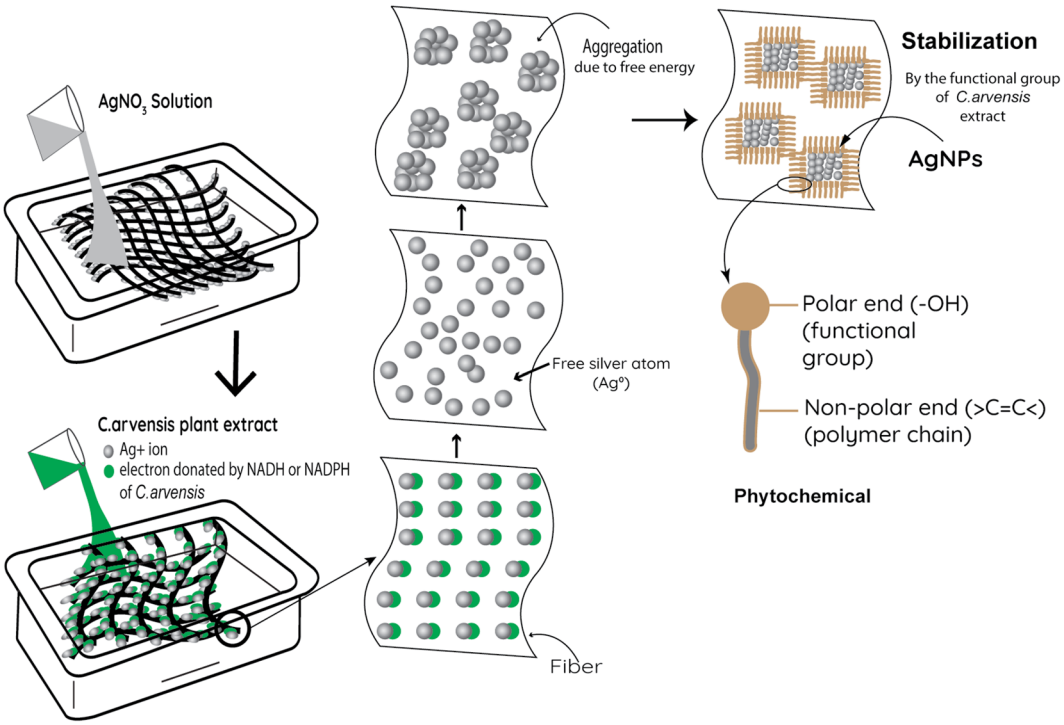

Fig. 2 In-situ method of green synthesis

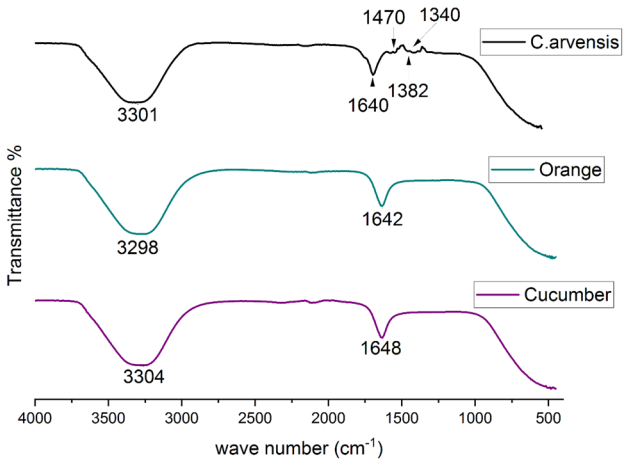

Fig. 3 FTIR of *C. arvensis*, orange and cucumber extract

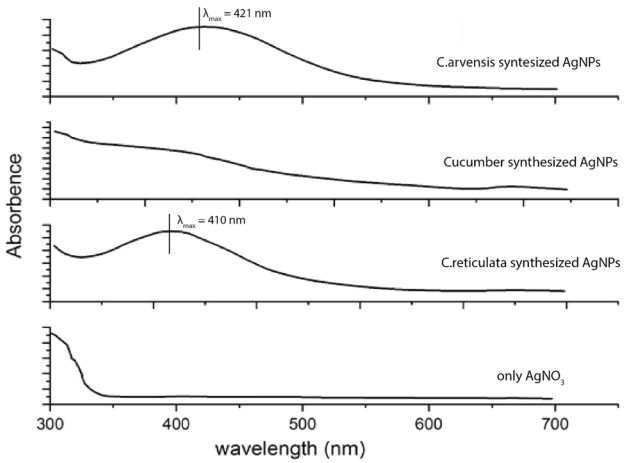

Fig. 4 UV–vis spectrum of different plant extract

Hence, aggregation after a certain limit must have to be prevented, which is termed as capping. Here, the recently shaped AgNPs continuously dropped the solution concentration; the nucleation process stops when it passes the critical level. Short nucleation can ensure uniform size distribution [40]. In green synthesis, the polar end of the functional groups (–OH) attach to the nanoparticles and limits the aggregation [41] (shown in Fig. 2).

3.2 FTIR of the Plant Extract

The FTIR spectrums of different plant extracts showed that the *C. arvensis* plant extract has three more functional groups than that of *C. reticulata* (mandarin orange) and *Cucumis sativus* (cucumber). All samples showed two

strong peaks at around 3300 cm^{-1} and 1640 cm^{-1} (Fig. 3). The broad band ranged 3000—3700 cm^{-1} represent –OH group. The band range from 1675 to 1600 cm^{-1} represents Alkenes with (C–C=C) symmetrical stretch (for example, 1-propene) or Alkenyl C=C stretch [42].

On the other hand, in the "fingerprint" region (from 1500 to 800 cm^{-1}) only the *C. arvensis* plant extract showed a weak peak at around 1340 cm^{-1}. The band corresponds to the –CH group [43]. The weak peak at 1340 cm^{-1} indicates the trans-wagging band of $–CH_2$ [44], whereas the weak peak at 1470 cm^{-1} shows the presence of $–CH_3$ (methyl C–H) asymmetrical or symmetrical stretching. Again, the –CH bending at 1390–1380 represents the –CHO group [45]. Hence, *C. arvensis* extract shows at least 4 functional groups whereas the orange and cucumber extracts show only the –OH and > C=C < stretching (figure -3).

3.3 UV–Vis

The UV–visible spectra of the *C. arvensis*, *C. reticulata*, and *Cucumis sativus* (cucumber) extract synthesized AgNPs are illustrated in Fig. 4. The *C. arvensis* and orange peel extract showed clear peaks at 421 nm and 410 nm, respectively. On the other hand, cucumber peel extract synthesized AgNPs solution failed to form any peak in the UV–Vis spectrum. AgNPs produce a surface plasmon resonance (SPR) band in the range of 350–500 nm [46]. Hence, the UV–Vis spectrum of *C. arvensis* and *C. reticulata* confirmed the AgNPs formation. On the contrary, *Cucumis sativus* (cucumber) failed to form AgNPs.

3.4 XRD

The XRD pattern of AgNPs shows four and three intense peaks for *C. arvensis* and *C. reticulata*, respectively, at different 2θ values ranging from 20 to 80 (Fig. 5). According to our calculation, the crystallinity of *C. arvensis* and *C. reticulata* synthesized AgNPs are about 70% and 31%, respectively.

The figure depicts various lattice parameters (miller index) such as (021), (111), (002), and (130) for *C. arvensis* synthesized AgNPs and (022), (213), (114) are for *C. reticulata* synthesized AgNPs. They are indexed as orthorhombic and Tetragonal crystal systems, respectively. The average crystal size is 5.10 nm for *C. arvensis* synthesized AgNPs, and 3.1 nm for *C. reticulata* synthesized AgNPs. The crystal sizes were calculated by the Scherrer equation where $K = 0.90$ and $\lambda = 1.540598$ (CuKα)

$$D = \frac{K\lambda}{\beta\cos\theta}$$

The *d*-spacing is calculated using the Braggs law:

$$\lambda = 2d\sin\theta$$

The lattice constants (a, b, c) are different in most crystals. Therefore, the lattice constants were calculated by using the following formula.

$$\frac{1}{d_{hkl}^2} = \frac{h^2}{a^2} + \frac{k^2}{b^2} + \frac{l^2}{c^2}$$

The calculated lattice parameters are very close to that of the reference (Table 2).

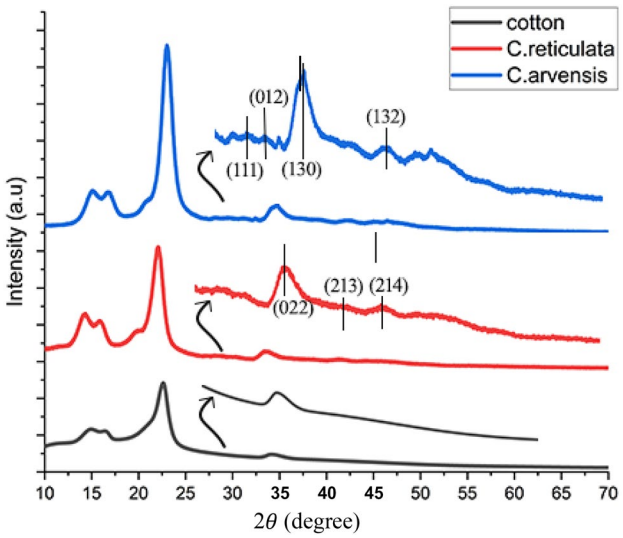

Fig. 5 XRD of *C. arvensis* and *C. reticulata* synthesized AgNPs

Table 2 XRD parameters for *C. arvensis* synthesized AgNPs

2θ	*hkl*	Micro-strain	Lattice *a*	Ref of lattice *a*	Lattice *b*	Ref of lattice *a*	Lattice *c*	Ref of lattice *a*
22.45	(012)	0.025796			10.75231	10.722		
28.786	(111)	0.004932						
30.786	(012)	0.03264					5.80399	5.851
34.020	(130)	0.03264	3.8812	3.864				

Fig. 6 SEM images for different methods

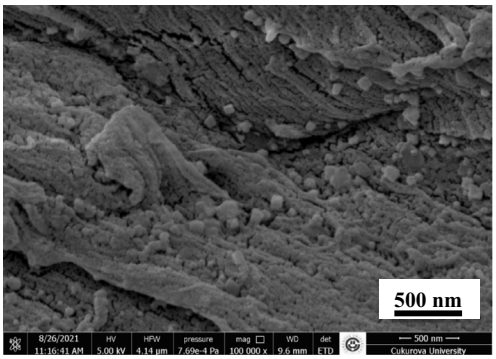

(a) *C.arvensis* synthesized AgNPs on plain fabric by immersion

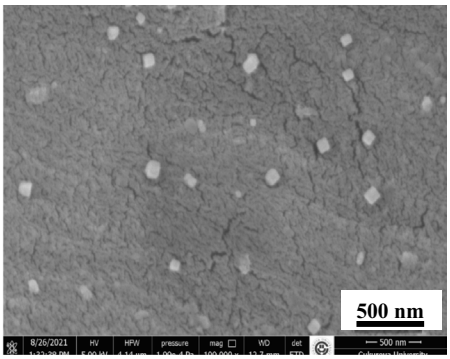

(b) *C.arvensis* synthesized AgNPs on plain fabric by In-situ method

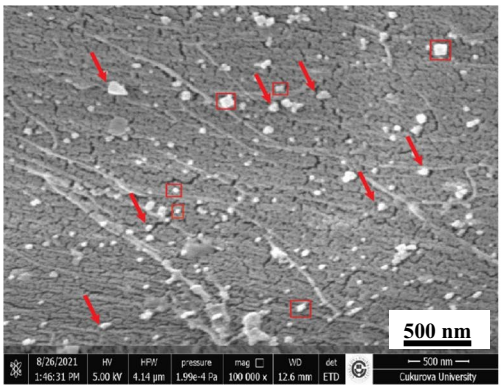

(c) *C.arvensis* synthesized AgNPs (from 0.009 M) on plain fabric by In-situ plain

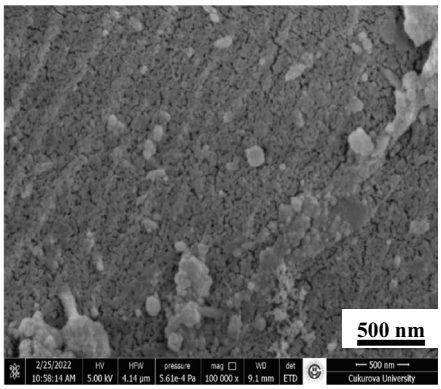

(d) *C.arvensis* synthesized AgNPs on twill fabrics by in-situ method

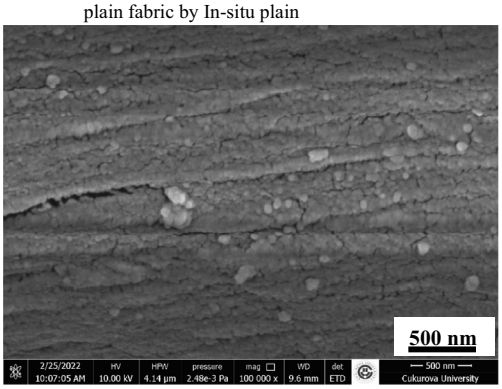

(e) *C.arvensis* synthesized AgNPs on plain fabric (by in-situ method)

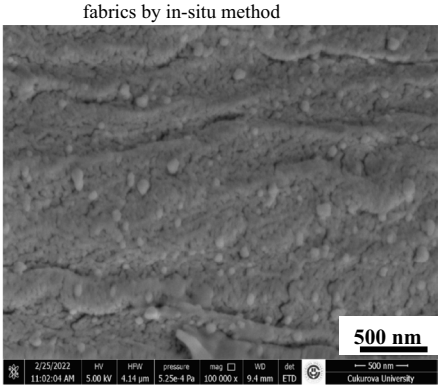

(f) *C.reticulata* peel synthesized on twill fabric by in-situ method

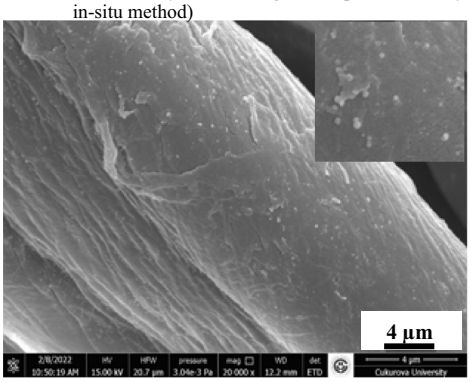

(g) *C.reticulata* peel synthesized on plain fabric by immersion method

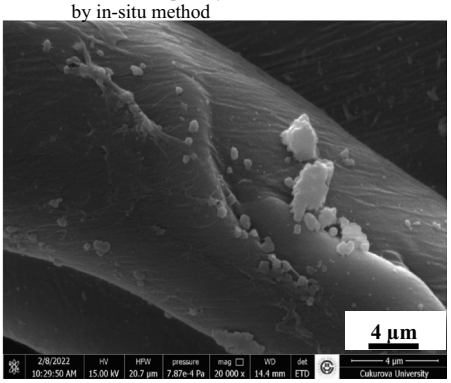

(h) *C.reticulata* peel synthesized on twill fabric in in-situ

Table 3 Shapes of different plant extracts

Plant extract	shape	$AgNO_3$	Nanoparticle size	References
C. arvensis	Square	0.002 M	49 nm	This study
C. arvensis	Cubic	0.002 M	54 nm	This study
C. arvensis	Irregular	0.001 M	58 nm	This study
C. arvensis	Square, triangular, spherical	0.009	33 nm	This study
C. reticulata	Spherical	0.002 M	54 nm	This study
C. reticulata	Spherical	0.002 M	74 nm	This study
C. reticulata	Spherical	0.002 M	66 nm	This study
C. camphora leaves (0.5 g)	Quasi-spherical	50 ml $AgNO_3$ (1 mM)	64 nm	[53]
C. coriaria leaves centrifuged	Various shapes	$AgNO_3$	78–98 nm	[54]
Ocimum sanctum	Triangular	$AgNO_3$(0.002 M) 5 mL	42 nm	[55]
Aloe vera leaf	Spherical	$AgNO_3$	20–25 nm	[20]
E. prostrata	Various shapes	$AgNO_3$ (1 mM) 88 mL	45 nm	[56]
Memecylon edule	Various shapes	$AgNO_3$ (10–3 M) 15 mL	50–90 nm	[57]
Curcuma longa (powder and extract)	Quasi-spherical triangular, small rod-shaped	$AgNO_3$ (50 mL of 1 mM)	71–80 nm	[58]
Annona reticulata	Spherical	$AgNO_3$ 0.1 M 9 mL	7.67–8.34	[59]
A. squamosa	Spherical	90 mL, 1 mM $AgNO_3$	20–100 nm	[60]
Neem/Salep	Star-like	45 mL, 1 mM $AgNO_3$	–	[61]
Neem leaves boil	Spherical	1:4 ratio to neem solution 0.01 M AgNO3	10–20 nm	[62]
Neem	Spherical and polydisperse	45 mL of 10^{-3} M aqueous $AgNO_3$	5–35 nm	[63]
C. zeylanicum (cinnamon) 2.5 g	Decahedral	50 mL of 1 mM aqueous $AgNO_3$	31–40 nm	[64]
Honey	Spherical	Less than 4 mL (0.1 N) $AgNO_3$	10 nm	[65]
A. alternata	Spherical	$AgNO_3$ (1–5 mM)	25–30 nm	[66]
Olive leaf	Spherical	$AgNO_3$	40 nm	[67]
Thymus kotschyanus	Spherical	$AgNO_3$	50–60 nm	[68]

3.5 SEM and EDS

To observe the shape and size of *C. arvensis* leaf and *C. reticulata* peel extracts synthesized silver nanoparticles (AgNPs), SEM and EDS were recorded. Most of the SEM images were taken at 100,000 magnification. The *C. arvensis* synthesized AgNPs were of different shapes such as cubic (Fig. 6a), square (Fig. 6b), triangular (shown in red arrow, Fig. 6c), square (shown in red square, Fig. 6c), irregular (Fig. 6d), nearly spherical (Fig. 6e), depending on various parameters including fabric types, incorporation methods, plant extract, and $AgNO_3$ concentration etc. On the contrary, the *C. reticulata* peel extract only produced nearly spherical shapes irrespective of all parameters (Fig. 6f–h). The acidic nature of *C. reticulata* extract minimizes the alkalinity of NaOH pretreatment and then it plays a crucial role in determining AgNPs shape. In this way, the AgNPs will be spherical. On the other hand, *C. arvensis* plant extract does not minimize the alkalinity of NaOH pretreatment at that extent, hence, various shapes will be produced here.

The average nanoparticle sizes of *C. arvensis* synthesized AgNPs range from 33 to 58 nm whereas the *C. reticulata* synthesized AgNPs's shapes are around 54 nm.

3.6 AgNPs Morphology Comparison

Various plant extracts, including *C. arvensis* and *C. reticulata* synthesized nanoparticle shape and size, are depicted in Table 3. It shows the shape of *C. arvensis* synthesized AgNPs are significantly affected by the $AgNO_3$ molarity, incorporation method, fabric type, etc. On the contrary, irrespective of parameters, the *C. reticulata* peel extract constantly produced spherical or nearly spherical shapes. Additionally, other plant extracts produce spherical shapes in most cases, except for a few exceptions, such as neem/salep or Ocimum sanctum, which produced star-shaped and triangular-shaped nanoparticles. Cheon

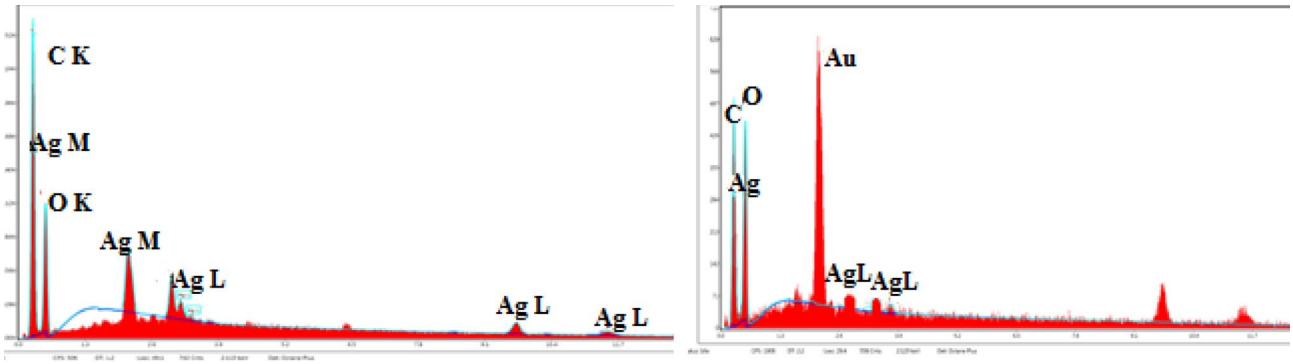

(a) EDS of C.arvensis synthesized AgNPs (b) EDS of C.reticulata synthesized AgNPs

Fig. 7 EDS of AgNPs incorporated fabrics

et al. [47] reported antibacterial activity of AgNPs largely depends on the shape due to its relation to the Ag ions release. [48] showed cubic shape has highest antibacterial activity among nanocubic, nanospherical and nanowires. Truncated triangular AgNPs outperformed spherical or rod shaped AgNPs [49]. Different shapes have different surface areas and active facets of AgNPs [50]. The non-spherical shapes are highly desirable for good antibacterial efficiency [51].

Furthermore, the *C. arvensis* synthesized AgNPs have a size range between 33 to 54 nm, whereas the *C. reticulata* peel extract produced 54–74 nm. Neither *C. arvensis* nor *C. reticulata* synthesized nanoparticle size was not as small as hone synthesized, or neem leaves synthesized nanoparticles (Table 3). Smaller nanoparticles are significant for excellent antimicrobial action [52]. However, the size range of *C. arvensis* and *C. reticulata* plant extract synthesized AgNPs are good enough for antibacterial properties.

3.7 EDS

Both *C. arvensis* and *C. reticulata* extract synthesized AgNPs. The EDS spectrum (Fig. 7) has different peaks for Ag, C, O the EDS profile shows Ag peaks which confirm that the AgNPs were formed in the reaction medium in both images. Further, at around 3 keV, some peaks are typically caused by the absorption of silver nanocrystals due to the surface plasmon resonance of AgNPs [69]. The C and O elements indicate the presence of carbon and oxygen in *C. arvensis* plant extract and cotton fiber. Other strong peaks are from Au due to the gold plating of the sample before SEM sample preparation. The K and L beside the metal elements represent the shell of the metal.

3.8 Antibacterial activity

Although the exact mechanism of AgNPs's antibacterial activity is not clear, but it can be hypothesized that the continuous releases of Ag^+ from AgNPs is mainly responsible for antibacterial activity. The Ag^+ adhere to the cell wall and cytoplasmic membrane is due to the electrostatic attraction and affinity to sulfur proteins [70].

You et al. [71] described in details of antibacterial mechanisms. Some researchers believe smaller silver nanoparticles (AgNPs) penetrate the microbes and release Ag^+ in cytoplasm which destroy the intracellular structure.

Gordon et al. [72] synthesized nano structured coating by silver polymer coordination polymer and demonstrated Ag^+ binds thiol groups in amino acid and expedite the Ag^+ release and –OH radical formation mediated by reactive oxygen species (ROS). They recommended that the enzyme inactivation by Ag^+ to thiol group binding is the key to antibacterial activity. Su et al. [73] observed silver-clay nanohybrids adherence on bacterial cell from scanning electron microscope (SEM) images. But, the nanohybrids are unable to penetrate, latter the nanoparticles initiate cell death by generating ROS.

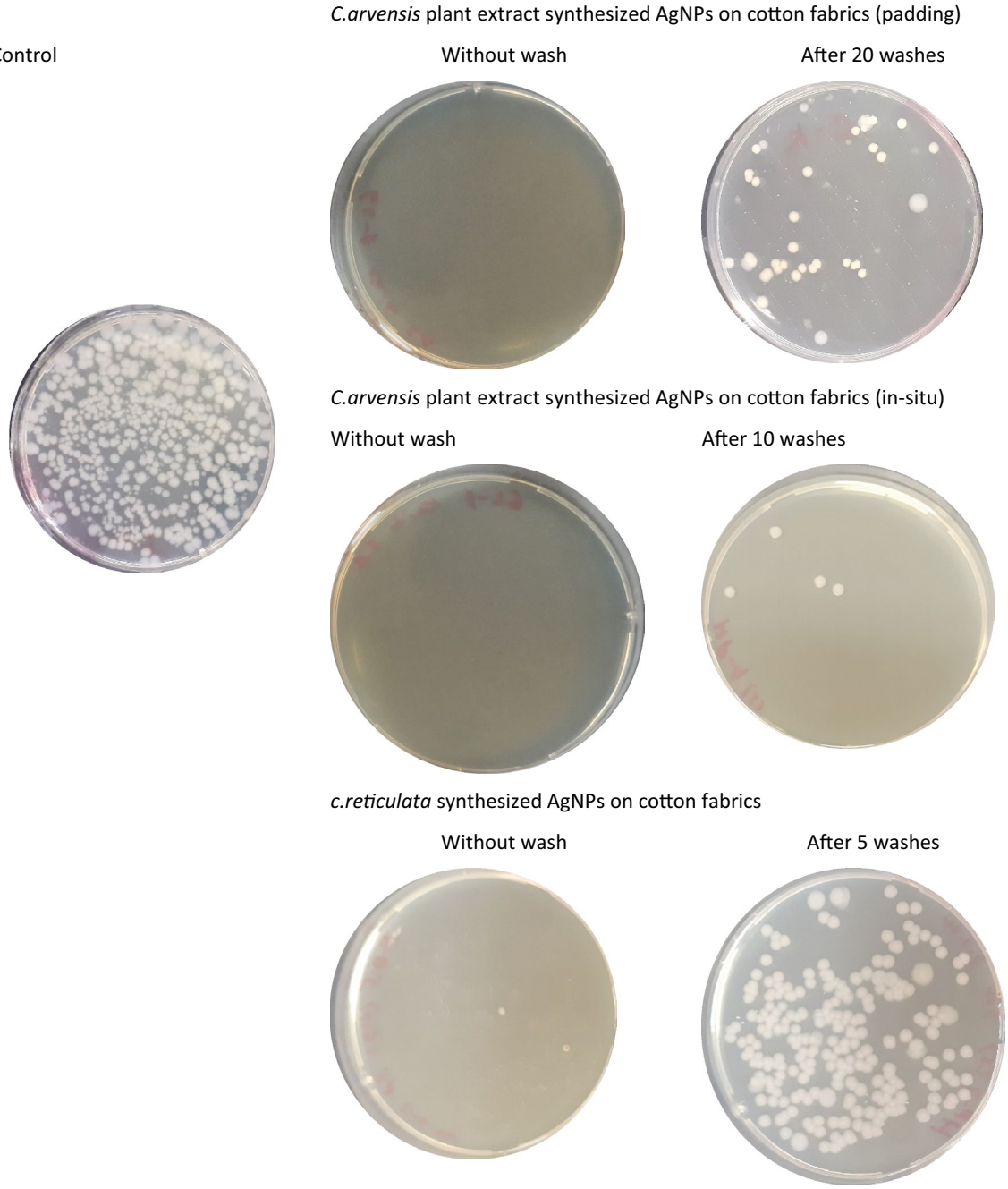

3.9 C. arvensis on Wash Fastness

Wash fastness is a crucial factor of antibacterial textiles. The leaching of Ag^+ or AgNPs may cause pollution. Simultaneously, it reduces the antibacterial activity of the AgNPs incorporated textiles. Unfortunately, AgNPs cannot create any chemical bond with the cellulosic fibers. Hence mechanical bonding or entrapping is the principal way of wash fastness.

Various researchers worked on increasing antibacterial wash fastness in various ways; some used binding agents, some used cross-linking agents, etc. The results of this study and previous related studies are depicted in Table 4. It shows the best performance came from *A. alternata* fungus, which shows almost full antibacterial properties even after 20 washes. However, butyl acrylic binder was used here. Among the samples without any binder, Honey synthesized

Table 4 Wash fastness of different green synthesized AgNPs

SL.	Plant	Loading method	Binder	Washes	Before wash	After wash	Loss	References
1	*C. arvensis*	Padding (2 times)	No	20	100%	96%	4%	This work
2	*C. arvensis*	Padding	No	10	100%	99%	1%	This work
3	*C. arvensis*	In-situ	No	10	100%	99%	1%	This work
4	*C. reticulata*	In-situ	No	5	100%	88%	12%	This study
5	Honey	Padding	No	10	100%	87%	13%	[65]
6	Honey	Padding	Printofix binder, (acrylate-based)	10	100%	98%	2%	[65]
7	*A. alternata* fungus	Immersion	Butyl acrylic binder	20	100%	99%	1%	[66]
8	Hydroxypropyl starch (HPS)	Padding	No	20	96%	62%	30%	[18]
9	Hydroxypropyl starch (HPS)	Padding	Binder: Printofix	20	96%	95%	1%	[18]
10	*Streptomyces laurentii* (from *Achillea fragrantissima* plants)	Padding	No	5	1.62 ± 0.15	0.97 ± 0.12	40%	[74]
11	*Streptomyces laurentii* (from *Achillea fragrantissima* plants)	Padding	No	10	1.62 ± 0.15	0.69 ± 0.1	57%	[74]
12	Marine- macro-Algae (Red and green algae) for polysaccharide	Padding	2% citric acid (CA)	10	100%	87%	13%	[75]
13	Marine-macro-Algae (Red and green algae) for polysaccharide	In-situ	1% acrylic binder	10	100%	95%	5%	[75]

AgNPs loading with padding showed 13% antibacterial property loss after 10 washes. On the contrary, we found *C. arvensis* synthesized AgNPs with 2 times padding exhibited 96% antibacterial activity even after 20 washes without any binder or cross-linker. The antibacterial activity loss here is only 4%. In contrast, the in-situ method for the same plant extract showed about 99% antibacterial activity after 10 washes, whereas the *C. reticulata* peel extract showed 12% antibacterial loss after 10 washes with the same method. Hence, the *C. arvensis* plant extract performed more than 12 times that of the *C. reticulata* peel extract for the same method.

Compared with other samples, it is obvious that the *C. arvensis* plant extracts have an extraordinary antibacterial property, especially when padded with 2 times. On the other hand, regarding shape, the AgNPs were capable of producing square, cubic, spherical and triangular shapes. Whereas the *C. reticulata* peel extract only produced spherical shapes.

4 Conclusion

The silver nanoparticle is a dominant antibacterial agent due to its large surface area, low concentrate $AgNO_3$ can be used as a precursor, a wide range of effectivity, etc. Among various synthesis methods, green synthesis is the most convenient as it is super simple, cheap, and eco-friendly. But, green synthesis of AgNPs depends on some parameters including temperature, plant extract types, etc. It was seen that the *C. sativus* (cucumber) peel failed to synthesize AgNPs, again, *C. arvensis* leaf extracts failed to synthesize AgNPs below 40 °C. By using Taguchi orthogonal array (L_{16}) optimum temperature was found 55 °C and 55–70 °C temperatures for plant extract and $AgNO_3$, respectively. The synthesized AgNPs were incorporated into the fabrics by padding, immersion, and in-situ method, but for antibacterial wash fastness evaluation, only in-situ and padding methods were considered. It was found both padding and *in-situ* methods performed well for *C. arvensis* leaf extract showing about 99% antibacterial efficiency after 10 washes. On the other hand, *C. reticulata* peel extract performed comparatively poorer showing 88% antibacterial efficiency after only 5 washes. Surprisingly, among the available previous investigations on antibacterial wash fastness of AgNPs incorporated cotton fabrics, *C. arvensis* leaf extract synthesized AgNPs performed best without any cross-linking agent or binder. The *C. arvensis* synthesized AgNPs showed 70% crystallinity, 5.10 nm crystal size, 31 nm-58 nm nanoparticle size, and various shapes (square, triangular, spherical, irregular, etc.). On the other hand, *C. reticulata* peel synthesized AgNPs showed 31% crystallinity, 3.1 nm crystal size, 54 nm nanoparticle size, and only spherical shapes.

From the FTIR analysis, it was seen *C. arvensis* has at least 4 functional groups whereas *C. reticulata* and *C. sativus* have only 2 functional groups. Due to these functional groups, the *C. arvensis* synthesized nanoparticles showed better antibacterial wash fastness. However, a detailed study is needed to investigate the exact reason. Again, further study is needed to investigate the reason behind the failure of AgNPs synthesis from *C. sativus* (cucumber) peel extract.

Author Contributions Supervision RTO, research plan, methodology, manuscript preparation. TA, antibacterial tests and review OG.

Funding This research was funded by Cukurova University Scientific Research Fund. Project No. FDK-2021-13527.

Availability of Data and Materials Not applicable.

Declarations

Conflict of interest The author declared no competing interests.

Consent to participate Not applicable.

Consent for publication Not applicable.

Ethics approval Not applicable.

References

1. L. Windler, M. Height, B. Nowack, Environ. Int. **53**, 62 (2013)
2. G. Zhao, S.E. Stevens, Biometals **11**, 27 (1998)
3. R. Li, J. Chen, T.C. Cesario, X. Wang, J.S. Yuan, P.M. Rentzepis, Proc. Natl. Acad. Sci. **113**, 13612 (2016)
4. S.R.K. Pandian, V. Deepak, K. Kalishwaralal, P. Viswanathan, S. Gurunathan, Braz. J. Microbiol. **41**, 805 (2010)
5. S. Nafisi, H.I. Maibach, in Cosmetic Science and Technology, ed. By Kazutami Sakamoto, Robert Y. Lochhead, Howard I. Maibach, Yuji Yamashita (Elsevier,2017), pp. 337–369
6. A. Olfati, D. Kahrizi, S.T.J. Balaky, R. Sharifi, M.B. Tahir, E. Darvishi, Inorg. Chem. Commun. **125**, 108439 (2021)
7. J.R. Peralta-Videa, Y. Huang, J.G. Parsons, L. Zhao, L. Lopez-Moreno, J.A. Hernandez-Viezcas, J.L. Gardea-Torresdey, Nanotechnol. Environ. Eng. **1**, 4 (2016)
8. G. López-Téllez, P. Balderas-Hernández, C.E. Barrera-Díaz, A.R. Vilchis-Nestor, G. Roa-Morales, B. Bilyeu, J. Nanosci. Nanotechnol. **13**, 2354 (2013)
9. T. Ahmed, R.T. Ogulata, J. Nat. Fibers **19**, 8463 (2022)
10. S. Ahmed, M. Ahmad, B.L. Swami, S. Ikram, J. Adv. Res. **7**, 17 (2016)
11. S. Kanchi, S. Ahmed (eds.), *Green metal nanoparticles: synthesis, characterization and their applications* (Wiley-Scrivener, Hoboken, 2018)
12. S. Pai, A. Hebbar, S. Selvaraj, Environ. Sci. Pollut. Res. **29**, 35518 (2022)
13. P.S. Vankar, D. Shukla, Appl. Nanosci. **2**, 163 (2012)
14. A.M. Awwad, N.M. Salem, A.O. Abdeen, Int. J. Ind. Chem. **4**, 29 (2013)
15. M. Maghimaa, S.A. Alharbi, J. Photochem. Photobiol. B **204**, 111806 (2020)
16. T. Ahmed, R.T. Ogulata, S. Sezgin Bozok, J. Text. Inst. **113**, 2825 (2022)
17. D. Zhang, L. Chen, C. Zang, Y. Chen, H. Lin, Carbohydr. Polym. **92**, 2088 (2013)
18. A. Hebeish, M.E. El-Naggar, M.M.G. Fouda, M.A. Ramadan, S.S. Al-Deyab, M.H. El-Rafie, Carbohydr. Polym. **86**, 936 (2011)
19. B. Tang, J. Kaur, L. Sun, X. Wang, Cellulose **20**, 3053 (2013)
20. Q. Zhou, J. Lv, Y. Ren, J. Chen, D. Gao, Z. Lu, C. Wang, Text. Res. J. **87**, 2407 (2017)
21. E. Ituen, E. Ekemini, L. Yuanhua, A. Singh, J. Mol. Struct. **1207**, 127819 (2020)
22. M. Hussain, N.I. Raja, Z. Mashwani, F. Naz, M. Iqbal, S. Aslam, IET Nanobiotechnol. **12**, 514 (2018)
23. P.K. Mukherjee, N.K. Nema, N. Maity, B.K. Sarkar, Fitoterapia **84**, 227 (2013)
24. R.K. Saini, A. Ranjit, K. Sharma, P. Prasad, X. Shang, K.G.M. Gowda, Y.-S. Keum, Antioxidants **11**, 239 (2022)
25. S.S. Ferreira, A.M. Silva, F.M. Nunes, Ind. Crops Prod. **111**, 141 (2018)
26. D. Arora, A. Rani, A. Sharma, Pharmacogn. Rev. **7**, 179 (2013)
27. H. Serví, C. Vatansever, A. Doğan, V. Majeed, Int. J. Second. Metab. **7**, 229 (2020)
28. H. Rodríguez-Acosta, J.M. Tapia-Rivera, A. Guerrero-Guzmán, E. Hernández-Elizarraráz, J.A. Hernández-Díaz, J.J.O. Garza-García, P.E. Pérez-Ramírez, S.F. Velasco-Ramírez, A.C. Ramírez-Anguiano, G. Velázquez-Juárez, J.M. Velázquez-López, Y.G. Sánchez-Toscano, S. García-Morales, M.M. Flores-Fonseca, D.E. García-Bustos, D.R. Sánchez-Chiprés, A. Zamudio-Ojeda, J. Tissue Viability **31**, 173 (2022)
29. A. Baghizadeh, S. Ranjbar, V.K. Gupta, M. Asif, S. Pourseyedi, M.J. Karimi, R. Mohammadinejad, J. Mol. Liq. **207**, 159 (2015)
30. A. Balciunaitiene, V. Puzeryte, V. Radenkovs, I. Krasnova, P.B. Memvanga, P. Viskelis, P. Streimikyte, J. Viskelis, Molecules **27**, 7700 (2022)
31. T. Ahmed, R.T. Ogulata, O. Gülnaz, Results Chem. **4**, 100462 (2022)
32. N. Abutaha, F.A. Nasr, A.-Z. Mohammed, A. Semlali, F.A. Al-Mekhlafi, M.A. Wadaan, Mol. Biol. Rep. **46**, 2187 (2019)
33. J. Paolini, T. Barboni, J.-M. Desjobert, N. Djabou, A. Muselli, J. Costa, Biochem. Syst. Ecol. **38**, 865 (2010)
34. E. Ruiz De Clavijo, Acta Oecol. **28**, 119 (2005)
35. H. Kırmızıbekmez, C. Bassarello, S. Piacente, C. Pizza, İ Çalış, Z. Für Naturforschung B **61**, 1170 (2006)
36. M. Guilger-Casagrande, R. de Lima, Front. Bioeng Biotechnol. **7**, 287 (2019)
37. S. Anil Kumar, M.K. Abyaneh, S.W. Gosavi, S.K. Kulkarni, R. Pasricha, A. Ahmad, M.I. Khan, Biotechnol. Lett. **29**, 439 (2007)
38. X. Peng, J. Wickham, A.P. Alivisatos, J. Am. Chem. Soc. **120**, 5343 (1998)
39. S. Li, Y. Shen, A. Xie, X. Yu, L. Qiu, L. Zhang, Q. Zhang, Green Chem. **9**, 852 (2007)
40. C. Burda, X. Chen, R. Narayanan, M.A. El-Sayed, Chem. Rev. **105**, 1025 (2005)
41. V.V. Makarov, A.J. Love, O.V. Sinitsyna, S.S. Makarova, I.V. Yaminsky, M.E. Taliansky, N.O. Kalinina, Acta Naturae **6**, 35 (2014)
42. J. Coates, in *Encycl. Anal. Chem.*, edited by R. A. Meyers (Wiley, Chichester, 2006), p. a5606
43. G. Haberhauer, B. Rafferty, F. Strebl, M.H. Gerzabek, Geoderma **83**, 331 (1998)
44. M. Mecozzi, L. Nisini, Infrared Phys. Technol. **101**, 119 (2019)
45. S. Banerjee, A. Misra, S. Chaudhury, B. Dam, J. Hazard. Mater. **367**, 215 (2019)
46. M. Ider, K. Abderrafi, A. Eddahbi, S. Ouaskit, A. Kassiba, J. Clust. Sci. **28**, 1051 (2017)
47. J.Y. Cheon, S.J. Kim, Y.H. Rhee, O.H. Kwon, W.H. Park, Int. J. Nanomed. **14**, 2773 (2019)
48. X. Hong, J. Wen, X. Xiong, Y. Hu, Environ. Sci. Pollut. Res. **23**, 4489 (2016)
49. S. Pal, Y.K. Tak, J.M. Song, Appl. Environ. Microbiol. **73**, 1712 (2007)
50. T.C. Dakal, A. Kumar, R.S. Majumdar, V. Yadav, Front. Microbiol. **7**, 2116 (2016)
51. M.R. Nateghi, H. Hajimirzababa, J. Text. Inst. **105**, 806 (2014)
52. J.R. Morones, J.L. Elechiguerra, A. Camacho, K. Holt, J.B. Kouri, J.T. Ramírez, M.J. Yacaman, Nanotechnology **16**, 2346 (2005)
53. J. Huang, Q. Li, D. Sun, Y. Lu, Y. Su, X. Yang, H. Wang, Y. Wang, W. Shao, N. He, J. Hong, C. Chen. **18**, 105104 (2007)

54. K. Jeeva, M. Thiyagarajan, V. Elangovan, N. Geetha, P. Venkatachalam, Ind. Crops Prod. **52**, 714 (2014)
55. Y. Subba Rao, V. S. Kotakadi, T. N. V. K. V. Prasad, A. V. Reddy, D. V. R. Sai Gopal, Spectrochim. Acta. A. Mol. Biomol. Spectrosc. **103**, 156 (2013)
56. G. Rajakumar, A. Abdul Rahuman, Acta Trop. **118**, 196 (2011)
57. T. Elavazhagan, K.D. Arunachalam, Int. J. Nanomed. **6**, 1265 (2011)
58. M. Sathishkumar, K. Sneha, Y.-S. Yun, Bioresour. Technol. **101**, 7958 (2010)
59. E. Parthiban, N. Manivannan, R. Ramanibai, N. Mathivanan, Biotechnol. Rep. **21**, e00297 (2019)
60. R. Vivek, R. Thangam, K. Muthuchelian, P. Gunasekaran, K. Kaveri, S. Kannan, Process Biochem. **47**, 2405 (2012)
61. A. Rohani Shirvan, S. Kordjazi, A. Bashari, J. Nat. Fibers **18**(10), 1472–1480 (2019)
62. A. Tripathy, A.M. Raichur, N. Chandrasekaran, T.C. Prathna, A. Mukherjee, J. Nanopart. Res. **12**, 237 (2010)
63. S.S. Shankar, A. Rai, A. Ahmad, M. Sastry, J. Colloid Interface Sci. **275**, 496 (2004)
64. M. Sathishkumar, K. Sneha, S.W. Won, C.-W. Cho, S. Kim, Y.-S. Yun, Colloids Surf. B Biointerfaces **73**, 332 (2009)
65. M.K. El-Bisi, H.M. El-Rafie, M.H. El-Rafie, A. Hebeish, Egypt. J. Chem. **56**, 187 (2013)
66. H.M.M. Ibrahim, M.S. Hassan, Carbohydr. Polym. **151**, 841 (2016)
67. M.M.H. Khalil, E.H. Ismail, K.Z. El-Baghdady, D. Mohamed, Arab. J. Chem. **7**, 1131 (2014)
68. M. Hamelian, M.M. Zangeneh, A. Amisama, K. Varmira, H. Veisi, Appl. Organomet. Chem. **32**, e4458 (2018)
69. P. Magudapathy, P. Gangopadhyay, B.K. Panigrahi, K.G.M. Nair, S. Dhara, Phys. B Condens. Matter **299**, 142 (2001)
70. I.X. Yin, J. Zhang, I.S. Zhao, M.L. Mei, Q. Li, C.H. Chu, Int. J. Nanomed. **15**, 2555 (2020)
71. C. You, C. Han, X. Wang, Y. Zheng, Q. Li, X. Hu, H. Sun, Mol. Biol. Rep. **39**, 9193 (2012)
72. O. Gordon, T. VigSlenters, P.S. Brunetto, A.E. Villaruz, D.E. Sturdevant, M. Otto, R. Landmann, K.M. Fromm, Antimicrob. Agents Chemother. **54**, 4208 (2010)
73. H.-L. Su, C.-C. Chou, D.-J. Hung, S.-H. Lin, I.-C. Pao, J.-H. Lin, F.-L. Huang, R.-X. Dong, J.-J. Lin, Biomaterials **30**, 5979 (2009)
74. A.M. Eid, A. Fouda, G. Niedbała, S.E.-D. Hassan, S.S. Salem, A.M. Abdo, H.F. Hetta, T.I. Shaheen, Antibiotics **9**, 641 (2020)
75. H.M. El-Rafie, M.H. El-Rafie, M.K. Zahran, Carbohydr. Polym. **96**, 403 (2013)